ADVANCED ENGINEERING MATERIALS

DOI: 10.1002/adem.201500295

Programmable Elastic Metamaterials**

By *Babak Haghpanah, Hamid Ebrahimi, Davood Mousanezhad, Jonathan Hopkins* and *Ashkan Vaziri**

We introduce a novel concept for the design of programmable-elasticity metamaterials; materials whose elastic properties can be modified instantaneously and reversibly on demand. Real-time tunable linear and nonlinear elastic moduli are obtained in lattice materials by adjustment of strut connectivity via actuation of embedded electromagnetic locks. The Young's modulus and Poisson's ratio of prototype 2D materials are varied instantaneously by more than 2 orders of magnitude and between 0.15 and 0.9, respectively. The buckling strength of the structure is altered by an order of magnitude between two bifurcation states associated with a centrosymmetric and an anti-chiral buckling pattern.

1. Introduction

The reversible, real-time control of the elastic moduli of a material could enable a number of future technologies. Some foreseeable applications include morphing metamaterials, expandable biomedical devices, soft robotics, vibration isolators, and acoustic metamaterials. The potential for modification of elastic modulus has been previously reported for some homogenous solid materials such as metallic oxides,[1] polymers,[2,3] ultra-high temperature ceramics,[4] and shape memory alloy or polymer structures[5–7] subjected to a varying temperature field. However, the maximum amount of increase in elastic modulus in these materials is generally less than an order of magnitude. More complex material systems providing a wider range of tunability include magnetic particle loaded elastomers under an external magnetic field,[8–10] particle jamming mechanisms activated by vacuum pressure,[11,12] fluidic flexible matrix composites under hydraulic pressure,[13] beams with electrostatically tunable bending stiffness,[14,15] soft-matter composites embedded with channels of magnetorheological fluid and activated by magnetic field,[16] and elastomers embedded with a low-melting-point metal and a soft-matter resistance heater.[17] In spite of these advances in achieving tunable elasticity, existing technical limitations such as limited range of achievable modulus or relatively slow response time impede commercialization of materials with real-time elastic control. Moreover, the need for varying ambient temperature or magnetic fields as external stimuli, or the need for hydraulic/pneumatic actuation using pumps, valves, and fluid channels in these materials lessens the interest and feasibility of employing the proposed structures as real-time tunable elasticity options for versatile design and application.

Here, we propose an elegant concept for controlling the linear and nonlinear elastic properties of lightweight cellular materials by several orders of magnitude, using electrically switched electromagnetic engagement at certain locations within the cellular solid. The control of linear elastic properties is obtained through the real-time adjustment of the strut connectivity of lattice materials (Figure 1A, B), displaying a wide range of moduli between a fully bending-dominated incompressible network and one which is fully stretch-dominated. The adjustment over nonlinear elastic (i.e., post-buckling) behavior in a lattice material (Figure 1C) is achieved by altering the natural deformation mode of the lattice and forcing it to buckle in a pre-selected mode with higher strain energy through switchable electromagnetic interactions.

2. Programmable Linear Elastic Properties

Two 2D orthotropic lattice structures with real-time control of Young's modulus and Poisson's ratio were proposed and

[*] *Prof. A. Vaziri, Dr. B. Haghpanah, H. Ebrahimi D. Mousanezhad*
Department of Mechanical and Industrial Engineering, Northeastern University, Boston, Massachusetts 02115, USA
E-mail: vaziri@coe.neu.edu
Dr. B. Haghpanah, Prof. J. Hopkins
Department of Mechanical and Aerospace Engineering, University of California Los Angeles, Los Angeles, California 90095, USA

[**] *The authors would like to thank Dr. Jim Papadopoulos for many fruitful discussions and the idea of using compression blocks to give the cell walls in a beam structure one-sided bending stiffness. This work was supported by the United States National Science Foundation's Civil, Mechanical, and Manufacturing Innovation Grant No. 1149750. (Supporting Information is available online from Wiley Online Library or from the author.)*

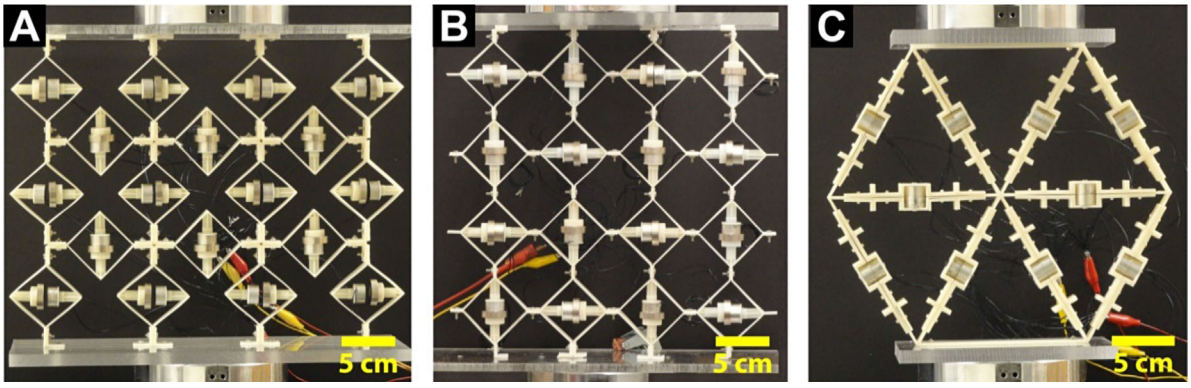

Fig. 1. Sample 3D printed programmable lattice materials with real-time control of (A) orthotropic Young's modulus, (B) orthotropic Poisson's ratio, and (C) buckling strength. The specimens were made from VeroWhitePlus material with Young's modulus of 2 GPa, Poisson's ratio of 0.35 and tensile strength of 55 MPa. The electromagnets used had a holding force of 5.5 lbs and response time of about 4 ms.

studied experimentally and analytically. The proposed cellular material with real-time tunable stiffness, shown schematically in Figure 2A, consists of an array of switchable stiffness units which are positioned in the middle of sides of an underlying square grid in alternating vertical and horizontal orientations. These units function as springs with a switchable spring constant. Each switchable stiffness unit, shown in Figure 2B in a "vertical" orientation, consists of four oblique beams and two transverse beams, which originate from the vertices of each pair of oblique beams and are connected through two electromagnets in the middle of the unit. The square-based grid has a fourfold symmetry and therefore possesses orthotropic material behavior.

In mode 0 of actuation (i.e., electromagnets deactivated), the Maxwell stability criterion requires the loaded unit to be both statically and kinematically indeterminate and deform by bending of edges when loaded according to $M = 2j - b - 3 = 2 \times 4 - 4 - 3 = 1 > 0$, where b and j are the number of struts and frictionless joints in the unit, respectively, and M is the number of inextensional mechanisms of the unit cell.[18] In mode 1 of actuation (i.e., electromagnets activated), however, the switchable stiffness unit is a properly triangulated frame with stretch-dominated behavior since $M = 2j - b - 3 = 2 \times 4 - 5 - 3 = 0$, and is much stiffer because the transverse bar carries tension. The effective orthotropic Young's modulus in compression of the lattice material in Figure 2A can be calculated as $E_0 = \frac{Et^3}{L^3 \sin^2\theta}$ and $E_1 = \frac{Et\cos^2\theta}{L(1+2\sin^3\theta)}$ for the case where all the switchable units are in modes 0 and 1 of actuation, respectively, where E is the elastic modulus of lattice cell wall material and θ, t, and L are the angle from vertical line, thickness, and length of the oblique beams (see the Supporting Information part A for detailed derivation of the elastic moduli of the lattice material in the two actuation modes). For the lattice material shown in Figure 1A with $t/L \simeq 0.045$ and $\theta = 45°$, the stiff-to-soft modulus ratio is obtained theoretically as $E_1/E_0 = 72$, which is in reasonable agreement with the ratio of $E_1/E_0 = 56$ from the experimental data (Part E of the Supporting Information provides details of the experimental investigation in this study). The discrepancy between analytical and experimental results is possibly due to the nonlinear/anisotropic behavior of 3D printed cell wall material and the contribution of shear strain energy which has been neglected in derivation of the analytical formula. Figure 2C shows the loaded lattice under uniaxial compression along y when all the electromagnets are activated (left) and deactivated (right).

Although the uniform actuation of switchable stiffness units results in discrete values of effective stiffness, the selective actuation of electromagnets in the lattice material can be used to obtain a nearly continuous range of effective elastic moduli. To estimate the stiffness under vertical compression, the pattern of activation for the *vertical* switchable stiffness units in the square-based structure shown in Figure 2A is assumed to be periodic and according to the Cartesian tiling of the m-by-n matrix C, called the representative volume element (RVE) of the structure. As a result, the stiffness of the structures is approximated by the effective stiffness of the RVE. Given that the binary value of actuation for a unit located in column i and row j of the RVE is represented by C_{ij}, the effective stiffness of the RVE, denoted by E_y^{eff}, can be estimated as

$$\sum_{j=1}^{n}\left(\sum_{i=1}^{m}\left(\frac{m\left(E_0 + C_{ij}(E_1 - E_0)\right)}{n}\right)^{-1}\right)^{-1} \le E_y^{\text{eff}} \le \left(\sum_{i=1}^{m}\left(\sum_{j=1}^{n}\frac{m\left(E_0 + C_{ij}(E_1 - E_0)\right)}{n}\right)^{-1}\right)^{-1} \quad (1)$$

where the lower- and upper-bounds in this relationship are obtained assuming the strain field to be uniform in x- and y-directions, respectively. The effective compressive orthotropic Young's modulus of the structure in the general case falls between the two extremes of the purely bending-dominated modulus, E_0 (i.e., $C_{ij} = 0; 1 \le i \le m,\ 1 \le j \le n$), and the purely stretch-dominated modulus, E_1 (i.e., $C_{ij} = 1; 1 \le i \le m,\ 1 \le j \le n$). The effective stiffness in stretching- and

ADVANCED ENGINEERING MATERIALS

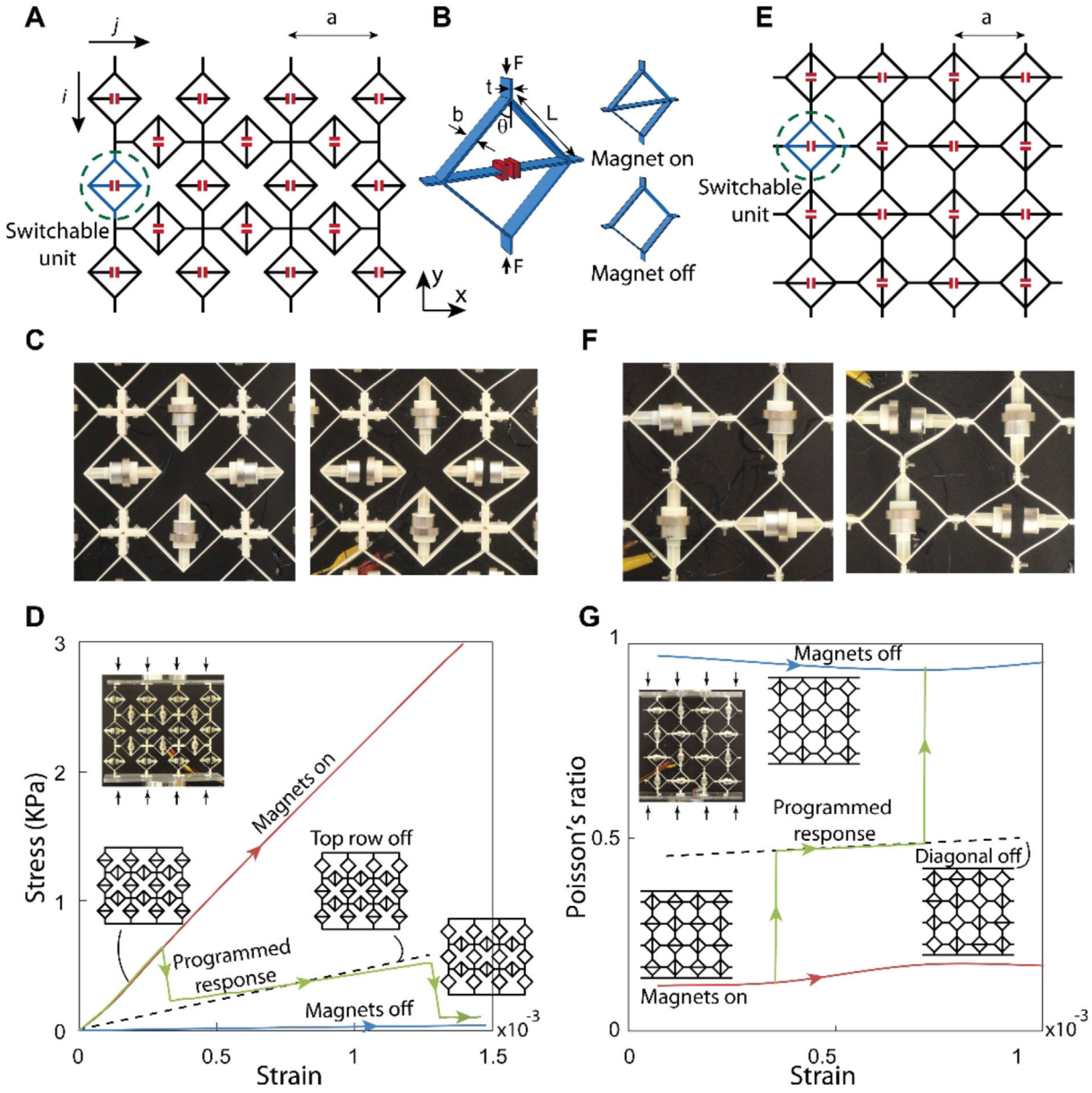

Fig. 2. Lattice materials for programmable linear elastic properties. (A, E) Schematics of square-based lattice materials equipped with real-time switchable units for the control of orthotropic Young's modulus and Poisson's ratio, respectively, (B) schematic of unit cell with programmable stiffness and lateral expansion, (C, F) the loaded lattice under uniaxial compression along y when all the electromagnets are activated (left) and deactivated (right), (D, G) corresponding plots of mechanical response for three different programmed paths. The red and blue lines show the cases where all the electromagnets are on and off, respectively. The dashed lines in (D, G) correspond to the lattice material where electromagnets on the top row of the lattice and on the diagonal were deactivated, respectively. The green line corresponds to a programmable response in each plot. In (D), the programmed response starts from the stiff response and transition to an intermediate response at a strain $\approx 0.3 \times 10^{-3}$ by deactivating the four electromagnets in the top row of the lattice material, and eventually to a soft response where all electromagnets are deactivated. In (G), the programmed response of the lattice under axial compression starts with all the magnets in the activated mode, resulting in small expansion in the transverse direction. At a strain $\approx 0.4 \times 10^{-3}$, the magnets on the diagonal of the lattice were deactivated and the material follows an intermediate response. This is followed by a transition to a nearly incompressible response, when all the magnets are deactivated at a strain $\approx 0.7 \times 10^{-3}$.

bending-dominated periodic 2D structures is proportional to the relative density of the structure and its cube, respectively.[19] As a result, the value of Young's modulus, given in (1), can be instantaneously changed over 2–4 orders of magnitude in low-density cellular materials (i.e., $t/L \ll 1$). [19]

The actual stress–strain response of a prototype structure under displacement-controlled vertical compression is shown in Figure 2D. The loading was applied using an Instron tester at a strain rate of $5 \times 10^{-5} s^{-1}$. The structure's response when all the electromagnets are deactivated or activated and also a *programmed* response are plotted in Figure 2C. In the programmed response, a purely stretching-dominated deformation mode (i.e., all electromagnets activated) is followed until $\varepsilon = 3 \times 10^{-4}$. At this compression level, all three vertical switchable stiffness units in the first row are deactivated, resulting in the separation of the electromagnets and a sudden drop in load. An intermediate path is then followed

until $\varepsilon = 1.3 \times 10^{-3}$, where the electromagnets are entirely deactivated. A bending-dominated, soft response follows afterward.

Active control over the Poisson's ratio was achieved using a similar tessellation of switchable units as shown in Figure 2E. In this design, each switchable elasticity unit is located at the nodes of an underlying square grid. The units alternate from a vertical to a horizontal orientation in rows and columns within the periodic lattice to give the structure a geometrical fourfold symmetry and an equal response in the x and y directions. When all the electromagnets are deactivated, the vertical and horizontal units will show a bending- and stretching-dominated response under y -loading, respectively, and for a lattice with $\theta = 45^\circ$, the amount of lateral expansion in the lattice material will be almost equal to the axial contraction. In contrast, when all the electromagnets are activated the lattice material is entirely stretching-dominated with smaller lateral expansion. For $\theta = 45^\circ$, the effective Poisson's ratio for the periodic structure, ν_{yx}, can be expressed as ≈ 1 (i.e., nearly incompressible) and $\sqrt{2}/(1 + (a/L))$ in modes 0 and 1 of actuation, respectively (see the Supporting Information part B for analytical derivation of the effective Poisson's ratio in the two deformation modes). Figure 2F shows the loaded lattice under uniaxial compression along y when all the electromagnets are activated (left) and deactivated (right). In Figure 2G, the value of effective incremental Poisson's ratio, $d\varepsilon_x/d\varepsilon_y$, from experimentation is plotted versus the axial compression for various patterns of actuation. In a programmed response, the behavior is switched suddenly from a state with Poisson's ratio ≈ 0.15 to an intermediate state with Poisson's ratio ≈ 0.5 by deactivating the electromagnets on the specimen's diagonal. This is followed by switching to a nearly incompressible behavior by deactivating all the electromagnets.

There are a few technical limitations associated with the exploratory designs shown in Figure 2A and E. First, the ability to control stiffness does not hold under macroscopic *tensile* stresses in these designs. In a periodic structure under tensile loading along x or y, the electromagnets in the switchable units that are oriented perpendicular to the loading direction are compressed against each other and a stretch-dominated response ensues. Second, the stiff-mode strength of the material under compression is limited to the tensile holding force of the electromagnets oriented perpendicular to the loading direction. Third, programmable softening would always be associated with a drop in load during displacement control experiments (or a sudden increase in displacement in load control experiments). This dynamic effect could lead to a destabilization in system's response. Finally, it is not possible to increase the effective stiffness at nonzero strains: once a soft response (electromagnets off) is selected at a switchable stiffness unit under loading, the magnet faces will separate and the unit loses its ability to follow a stiff response until the structure is fully unloaded and the magnets become close enough to attract each other.

The chart given in Figure 3A summarizes and compares the characteristics and functionalities of the previously introduced binary switchable unit and an alternative collinear locking mechanism capable of continuous gripping function. In the new design shown on the right, the pair of electromagnets in the original switchable unit is replaced with a lockable sliding mechanism which allows a free continuous relative contraction or extension of the two transverse beam segments in mode 0 and prevents this relative motion in mode 1 of actuation. Additionally, the locking mechanism can allow a relative extension or contraction of the two transverse beam segments at a constant force value (Part C of the Supporting Information provides details on the collinear locking mechanism designed and used in this study). This proposed design allows the periodic lattice material to be programmed to follow a new series of programmable paths including programmed softening without stress drop, programmed hardening at nonzero strains, and dissipative hysteresis loop. Figure 3B shows the experimental data on sample programmed responses for a programmable cellular material using the proposed collinear locking mechanism. The range of achievable stress–strain paths in this design is limited to all nonwork-producing paths in the material workspace described by Equation 1.

3. Programmable Nonlinear Elastic Response

The concept presented in Figure 4 allows designing lattice materials with programmable nonlinear elastic response, where the large-deformation response of the material is altered by forcing the material to follow selected instability patterns. Figure 4A shows a schematic of a triangular lattice material with programmable nonlinear elasticity. Each cell wall, also shown in this figure, consists of two adjacent walls with electromagnets between them that resist separation by mutual attraction in the activated mode. Each wall is covered by u-shaped *compression blocks*, stacked only along its outer side with very small spacing. The compression blocks give a cell wall one-sided bending stiffness, so it can buckle and bulge *outward* (i.e., toward the covered side) more easily than it can do inward. The second moments of area of the cell wall in the outward and inward directions are denoted by I_{out} and I_{in}, ($I_{\text{in}} > I_{\text{out}}$). Figure 4B shows the stress–strain response of a finite prototype structure with $I_{\text{in}}/I_{\text{out}} = 12$, compressed along y, for various electromagnet activation patterns.

When the structure is compressed vertically, the oblique cell walls become subject to axial compression forces. When electromagnets are deactivated, the slender walls are able to buckle outward at low axial force, and the structure will develop a geometrical pattern with six-fold floral symmetry, see Figure 4C. However, when all electromagnets are activated, axial buckling of the cell walls is suppressed, and the lattice material buckles at a higher load into an anti-chiral pattern observed in a regular triangular grid.[20] The stress corresponding to the onset of instability for the anti-chiral pattern was approximately 3.38 higher than that of the floral pattern. This is consistent with the theoretical prediction for

ADVANCED ENGINEERING MATERIALS

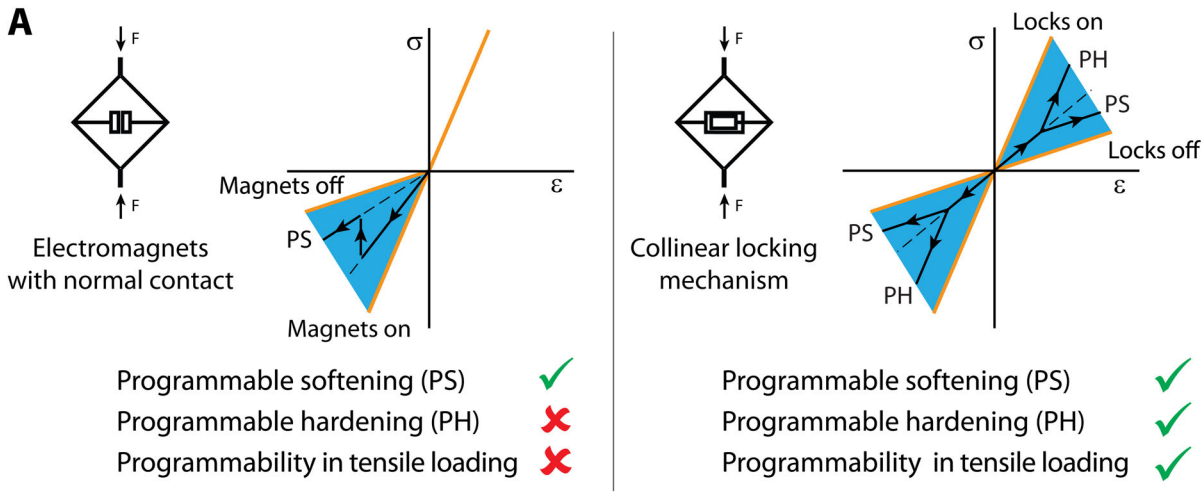

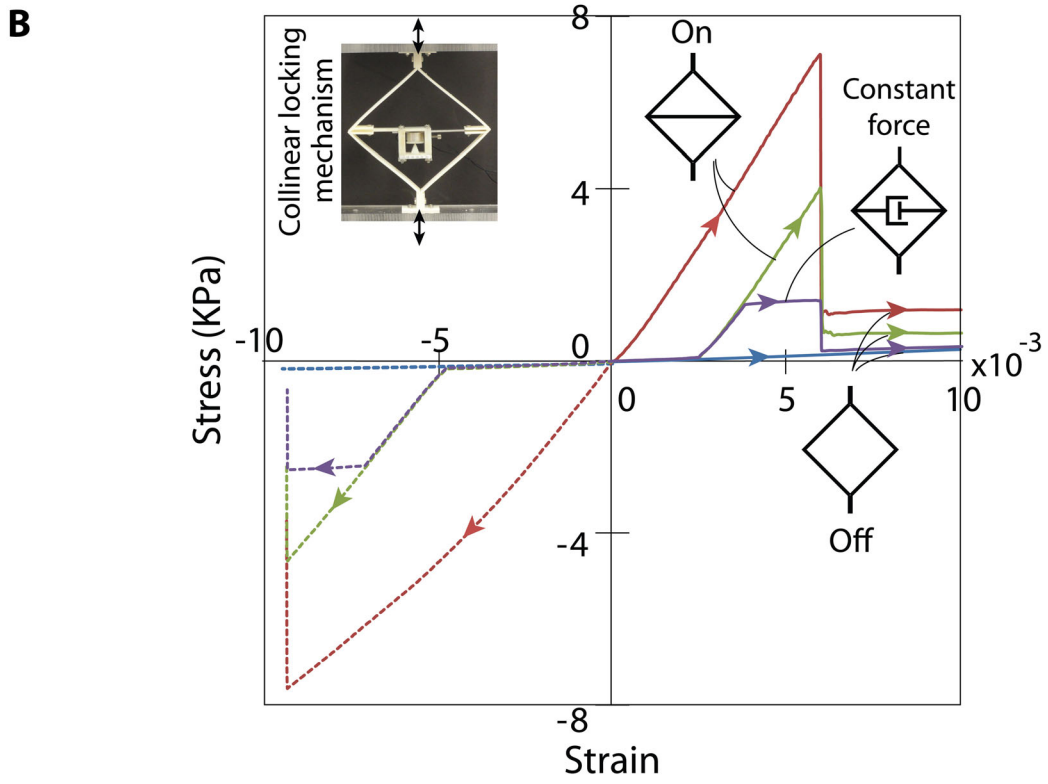

Fig. 3. Design concepts for the unit cell of programmable lattice material, (A) schematic demonstrations of the achievable paths (solids lines) in the axial stress–strain work-space (shaded area) for each concept. Compared to the original design (left), the proposed unit cell with collinear locking mechanism (right) enables a wider variety of programmed response including gradual hardening and gradual softening without stress drop in both tensile and compressive stress regions, (B) sample programmed stress–strain responses for a unit cell with collinear locking mechanism. The soft and hard responses are shown by blue and red lines, respectively. The green line shows a programmed response achieved by a bending-dominated response starting at zero strain and a hardening at a nonzero strain $\approx 2.5 \times 10^{-3}$ through a transition into a stretch-dominated response. The purple line shows a similar programmed response with a gradual hardening at strain $\approx 2.5 \times 10^{-3}$ and a gradual softening without stress drop at strain $\approx 3.9 \times 10^{-3}$ through a transition from stretch-dominated response into constant-force mode. The dashed lines show similar responses in the compression region.

the ratio of buckling strength of the periodic structure in the chiral (σ_0) and symmetric (σ_1) modes, $\frac{\sigma_0}{\sigma_1} = \frac{1}{4}\left(1 + \frac{l_{in}}{l_{out}}\right) = 3.25$ (see part D of the Supporting Information for the analytical derivation of buckling strength). Any activation pattern between these two states results in an intermediate response, such as case 2 studied in Figure 4C. Note that the proposed triangular structure should ideally have a unique linear elastic response. However, the pre-buckling response of the structure from the experiments is not unique and is dependent on the pattern of electromagnet actuation. This reliance of small-deformation response on the electromagnet activation pattern could be attributed to the initial curvature of the cell walls, primarily due to the weight of the electromagnets, which is ameliorated by activation of the electromagnets.

Despite possessing selectivity on a wide variety of buckling patterns, the proposed lattice offers limited mode

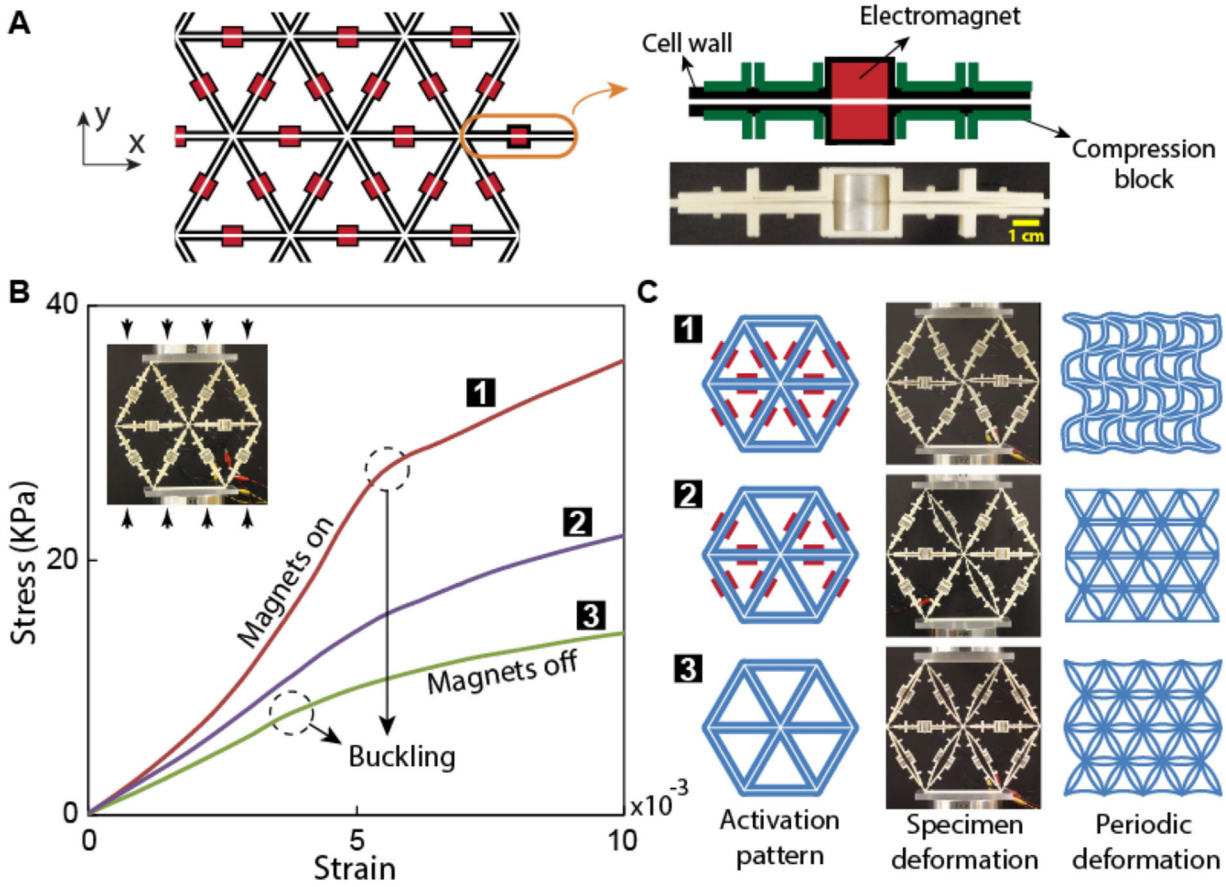

Fig. 4. Lattice material with programmable nonlinear elastic response. (A) Schematic of the triangular lattice material, where each wall is bi-layer and each layer is equipped with an electromagnet in the center (red) and is covered on the outer surface with compression blocks (green), (B) effective stress–strain response of a finite sample structure (inset) for three different electromagnet activation patterns, (C) electromagnet activation patterns for different curves in (B), with the activated electromagnets shown in red. The corresponding deformed shapes for finite specimens are shown in the middle pictures at strain of 0.01. Images on right show the idealized deformed shapes of infinite periodic structures for each electromagnet activation pattern. For an idealized infinite periodic structures, when all the electromagnets are activated (case 1), the lattice material buckles into a centrosymmetric pattern. When all the electromagnets are deactivated (case 3), the buckling shape becomes anti-chiral. Any activation pattern between these two states results in an intermediate response, such as case 2 studied here.

switch-ability. For instance, a switch from the floral mode to the unbuckled lattice shape is only possible at very small post-buckling deformations with minimal separation of the two cell wall layers where the electromagnets can effectively attract each other. The switch from the anti-chiral deformation to the floral deformation is only possible at strains smaller than $\varepsilon < 0.02$. Passing this level of compression, excessive bending in the cell walls will cause a geometric "lock" of the anti-chiral post-buckling deformation and prevent any mode change due to magnet de-activation.

4. Conclusion

The current study proposes robust pathways for the design of programmable materials capable of real-time, significant adjustment in their mechanical response. When combined with autonomous sensing and control strategies, these materials can be used in a new series of structural components with enhanced static and dynamic efficiency. The real-time adjustment of the strut connectivity within a lattice was shown to be a promising and effective way of achieving this goal. The use of lattices as the basis material has the additional benefit of yielding lightweight building materials for a diverse set of applications that impose significant penalties on mass. In the current study, the adjustment of strut connectivity is achieved via electromagnetic interactions inside the cellular solid. Reducing the size of electromagnets, which is generally associated with a more significant reduction in the electromagnetic efficiency, remains a significant hurdle toward reducing the cell size of the material in order to obtain such capability in micro- and nano-architected materials.

Article first published online: October 19, 2015
Manuscript Revised: September 21, 2015
Manuscript Received: June 9, 2015

[1] J. Wachtman Jr, W. Tefft, D. Lam Jr, C. Apstein, *Phys. Rev.* **1961**, *22*, 1754.
[2] R. Li, J. Jiao, Proceedings-Spie the International Society for Optical Engineering, International Society for Optical Engineering, Boston, MA **1999**, 068.

ADVANCED ENGINEERING MATERIALS

[3] F. Gandhi, S.-G. Kang, *The 14th International Symposium on: Smart Structures and Materials & Nondestructive Evaluation and Health Monitoring, International Society for Optics and Photonics*, San Diego, CA **2007**, 65251I.

[4] W. Li, R. Wang, D. Li, D. Fang, *Phys. Res. Int*. **2011**, 2011, article ID 791545.

[5] J. Rossiter, K. Takashima, F. Scarpa, P. Walters, T. Mukai, *Smart Mater. Struct*. **2014**, *23*, 045007.

[6] M. R. Hassan, F. Scarpa, M. Ruzzene, N. Mohammed, *Mater. Sci. Eng. A* **2008**, *481*, 654.

[7] G. Mcknight, R. Doty, A. Keefe, G. Herrera, C. Henry, *J. Intell. Mater. Syst. Struct*. **2010**, *21*, 1783.

[8] Z. Varga, G. Filipcsei, M. Zrínyi, *Polymer* **2006**, *47*, 227.

[9] S. Abramchuk, E. Kramarenko, D. Grishin, G. Stepanov, L. Nikitin, G. Filipcsei, A. Khokhlov, M. Zrinyi, *Polym. Adv. Technol*. **2007**, *18*, 513.

[10] T. Shiga, A. Okada, T. Kurauchi, *J. Appl. Polym. Sci*. **1995**, *58*, 787.

[11] E. Brown, N. Rodenberg, J. Amend, A. Mozeika, E. Steltz, M. R. Zakin, H. Lipson, H. M. Jaeger, *Proc. Natl. Acad. Sci*. **2010**, *107*, 18809.

[12] V. Trappe, V. Prasad, L. Cipelletti, P. Segre, D. Weitz, *Nature* **2001**, *411*, 772.

[13] Y. Shan, M. Philen, A. Lotfi, S. Li, C. E. Bakis, C. D. Rahn, K.-W. Wang, *J. Intell. Mater. Syst. Struct*. **2009**, *20*, 443.

[14] A. Bergamini, R. Christen, B. Maag, M. Motavalli, *Smart Mater. Struct*. **2006**, *15*, 678.

[15] M. Henke, J. Sorber, G. Gerlach, International Society for Optics and Photonics, San Diego, CA **2012**.

[16] C. Majidi, R. J. Wood, *Appl. Phys. Lett*. **2010**, *97*, 164104.

[17] W. Shan, T. Lu, C. Majidi, *Smart Mater. Struct*. **2013**, *22*, 085005.

[18] J. C. Maxwell, *London, Edinburgh, Dublin Philos. Mag. J. Sci*. **1864**, *27*, 294.

[19] L. J. Gibson, M. F. Ashby, *Cellular Solids: Structure and Properties*, Cambridge Univ. Press, Cambridge, UK **1999**.

[20] B. Haghpanah, J. Papadopoulos, D. Mousanezhad, H. Nayeb-Hashemi, A. Vaziri, *Proc. R. Soc. A* **2014**, *470*, 20130856.

